

Bi-Directional LSTM Model for Accurate and Real-Time Landslide Detection: A Case Study in Mawiongrim, Meghalaya, India

J Sharailin Gidon, Jintu Borah, *Member, IEEE*, Smrutirekha Sahoo, Shubhankar Majumdar, *Senior Member, IEEE*, and Masahiro Fujita, *Senior Member, IEEE*

Abstract—This paper presents a bi-directional Long Short-Term Memory (LSTM) model for the detection of landslides. Previous uses of machine learning in this setting have demonstrated its general potential, which necessitates the implementation of a suitable algorithm. Landslides are natural disasters that can cause significant destruction and disruption in the affected areas. Early detection is the key to minimizing the impact of landslides, so it is important to develop accurate and efficient models. An area selected for this study is located in Mawiongrim, Meghalaya, India, which is an active landslide zone. The proposed model uses a bi-directional LSTM to capture the temporal patterns of the input data collected from a long-term real-time monitoring system set up in the area. To evaluate the effectiveness of the predictions, the model is trained using a dataset composed of various landslide-related characteristics, such as topography, rainfall, hydrological and soil properties. The results show that the suggested model is capable of detecting landslides with greater accuracy and the lowest error value relative to other models. Additionally, the model is also able to provide a real-time warning system, making it a viable tool for early landslide detection. The research also highlights the prediction models for matric suction and groundwater level, which are crucial in determining slope stability.

Index Terms—Artificial Intelligence, Landslides, LSTM, Real-time Monitoring, Slope detection

I. INTRODUCTION

A Delicate slope in an area with frequent or persistent rainfall is more likely to cave in if the slope is already unstable. The slope will collapse when the changes in soil stress behaviour caused by rain infiltration reach a point greater than the soil shear strength. Without studying the movement patterns of landslides in response to certain climatic events, it is quite challenging to make accurate predictions of their occurrence [1]. Slope movement monitoring alone is insufficient; other elements like environmental and geotechnical features are essential. Based on a large data set demonstrating slope behaviour under the impact of rainwater infiltration, physical and empirical-based models may be simulated for a trustworthy warning system [2]. Several physical factors, including slope material, slope strength, subsurface water, rainfall infiltration,

J.S.Gidon and S.Sahoo is with the Dept. of CE at the National Institute of Technology Meghalaya, Shillong-793003, India (e-mail:sharailingidon@gmail.com)

J.Borah and S. Majumdar is with the Dept. of ECE, at National Institute of Technology Meghalaya and Shillong, Meghalaya 793003 India (e-mail: shubuit@gmail.com)

M.Fujita is with the VLSI Design and Education Center at University of Tokyo, Japan (e-mail:fujita@ee.t.u-tokyo.ac.jp)

and slope geometry influence slope stability. To comprehend the circumstances in which the slope might collapse, observing these aspects' activity is required. Seepage and deformation may be monitored concurrently with slope stability. It may aid in evaluating slope behaviour under various circumstances and give details on the effectiveness of the preventative strategy. Real-time monitoring may provide alerts on probable slope failures. The time-to-time change in these characteristics may be verified using various devices. Irrometers may be used to measure soil suction or negative pore water pressure. A piezometer may be used to track changes in the groundwater level. A rain gauge may be used to track changes in rainfall quantity and duration [3]. Inclinometers, Global Positioning System (GPS), total stations, piezometers, and other tools are often used in landslide monitoring techniques.

Throughout the last 50 years, a large number of prediction studies using artificial intelligence (AI) machine learning (ML) models have been created [4]. Advanced studies using recurrent neural networks, neural dynamics solvers, residual neural network-based non-negative latent factors, and sampling-based multilayer-structured latent factor (MLF) model [5]–[10] have been extensively used for data prediction. An advanced procedure was developed by providing a game-theoretic framework to guide the design of recurrent neural networks for the distributed coordination of numerous redundant manipulators. A time-delayed and distributed neural dynamics scheme was suggested in response to the collaborative control challenge of redundant manipulators with time delays [6]. A symmetric non-negative latent factor analysis (ASNL) model based on the alternating-direction method of multipliers (ADMM) was presented for accurately expressing the symmetry and effectively handling the incomplete data of large-scale undirected weighted networks [8]. AI-based models do not stop at manipulating or predicting manipulators, performance, machine translation, etc., but extend to predicting landslides and slope displacements. The primary indicator of the landslide progression process is slope displacement. Investigating and forecasting landslide displacement is crucial and advantageous to anticipate slope failures. This study focuses on the data collected from a site monitoring system that is one of a kind in the region of Meghalaya, India. The study of landslide prediction goes back to the 1960s [11], and one of the most related models is long-term memory (LSTM), which is a powerful RNN designed primarily to handle the exploding/vanishing problem gradient issues frequently occurring when learning

long-term dependency models. The LSTM model effectively uses the real-time information gathered locally to predict the slope movement of a region effectively. LSTM has since been improved upon and made more well-known by other researchers, including [12], [13] etc. Tests demonstrated this framework's robustness and superior performance compared to cutting-edge techniques. In the machine learning literature, recurrent neural network (RNN)-based long short-term memory (LSTM) has been established to predict soil movement [14], [15]. These recurrent models, an extension of feedforward neural networks, include internal memory. The current input results depend on previous computations in these recurrent models, which carry out the same function for every data input. Several academics created single-layer LSTM models to predict soil movement. These models used a time series of historical soil movements [15]–[18] to predict potential slope movements. To predict soil movements during known actual landslides in India's Himalayan areas, a bidirectional-stacked (BM) LSTM ensemble model was proposed [19]. It has proven effective to use the LSTM network for time-series analysis in prediction and recognition [20] when standard computational intelligence techniques fall short. Deep learning prediction models with a single component and many factors are implemented. [21] shows a performance evaluation of the deep learning model and discusses the factors that influence it.

According to previous research, most of them have high accuracy levels and highly significant root mean square errors. This indicates that the prediction models may have high mistakes when predicting the landslip occurrence. Therefore, the new study provides low error rates and highly accurate landslides or slope displacement predictions. In the present study, a prediction model for rainfall-induced landslides is developed using the RNN-based LSTM method. This model is chosen for its ability to predict long-term data. The slope data used in the model are parts of the real-time monitoring system set up in an area located in Mawiongrim, Meghalaya, India. The LSTM models are used to study the dependency of the slope displacement on the rainfall patterns, changing matric suction, and varying groundwater table during monsoon periods. The models also analyze the changing matric suction and groundwater level with rainfall. In the current study, a deep learning model is given for predicting slope inclinations and the area's matric suction and water level, which are critical factors in determining the possibility of landslide activities. Moreover, the models give the least errors compared to the other existing studies. Five slope inclination models (INC), three matric suction (MS), and water level (WL) have been developed.

II. BACKGROUND

Models based on physical principles and models based on data can be used to categorize these studies in general ([16], [22]). The development of deep learning, particularly with the advent of LSTM, has made it feasible to develop a trustworthy solution for time-series data with long-term dependencies. Time series analysis methods are often used

to research and create prediction models because landslide displacement requires typical time series data [15], [23]. The range of displacement values expected by landslide prediction models determines the forecast's accuracy rather than a single figure [24], [25], [17]. To directly predict landslide displacement while taking slopes, land use factors, landslide profiles, and rock characteristics of landslides into consideration, [26] employed the LSTM model. Displacement information from the models is one kind of data that may show the stability and changing status of the landslide itself over time [27]. To ascertain the displacement projection, this model is proved correct by contrasting the prediction's outcomes with the one-year total displacement measurement [26]. A variation mode decomposition VMD algorithm was developed using the LSTM model to dynamically model the periodic and stochastic slope displacements. However, VMD's performance is severely limited because the settings are typically chosen based on personal experience. In consideration of the nonlinear dynamic aspects of landslide displacement, the Bi-LSTM is used in order to investigate the displacements of step-like landslides. This technique is effective in capturing both the past and the future components of monitoring data [18]. Slope failure is caused by decreasing matric suction in soil, which causes a loss in soil strength. Hence, it is helpful to have information on rainfall parameters and their effects on soil shear strength, soil-water interaction, changing groundwater table, and how they contribute to landslides [28]. The Himalayas in Northwest and Northeast India and the Western Ghats in Peninsular India, are the areas where landslides are most likely to occur during rainfall season. Meghalaya is a state in the Northeastern part of India. Regarding landslides in Meghalaya, we have faced many calamities, especially due to intense rainfall.

LSTM Networks that are bidirectional [29] in the sequence tagging job since we have access to both previous and forthcoming input data at a certain moment in time. Because of this, we can effectively use features from the past (through forward states) and features from the future (via backward states) over a certain period. Backpropagation through time is the method that is used to train bidirectional LSTM networks [30]. Throughout time, forward and reverse sweeps across the unfurled network are made in a way comparable to the forward and backward passes carried out over a normal network, except that at each time step, we must reveal the hidden states. Also, we need a special approach for the data points' start and end. We make use of a batch implementation, which permits the processing of numerous phrases at the same time.

III. STUDY AREA

Mawiong Rim is a desolate region that can be found in Meghalaya, India, on the National Highway 6, Guwahati Shillong (GS) Route (Fig. 1). This region is notorious for its precipitous hillsides, deep valleys, and delicate bedrock, all contributing to the increased likelihood of landslides occurring here. Additionally, this region is well-known for its high rainfall, which is known to further contribute to the mountains' precarious stability. The infrastructure of Mawiong Rim is

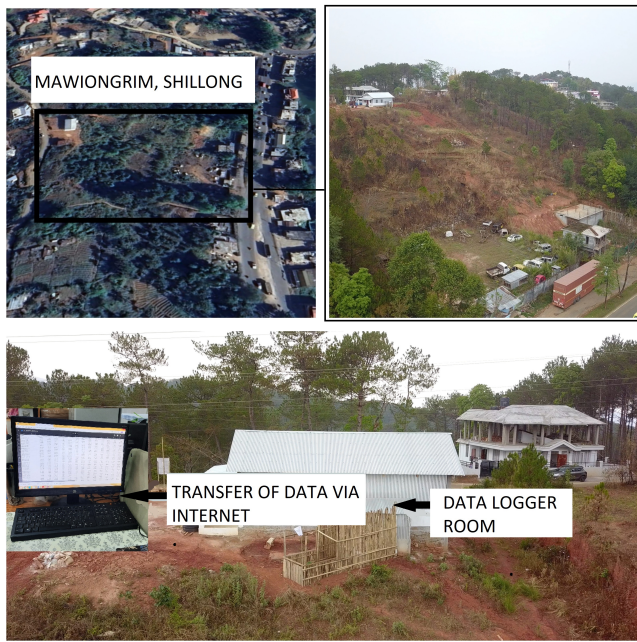


Fig. 1: Study area (i) Google Earth Map (ii) Aerial view (iii) Data logger location and mode of data transfer

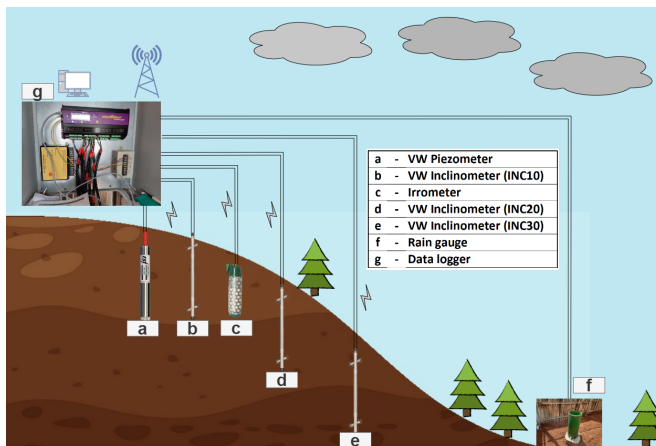


Fig. 2: Sensor system architecture and deployment for real-time monitoring

vulnerable to the natural danger of landslides, which can cause substantial damage to the area. This region is prone to sudden inundation, which can further destabilize the hillsides and cause landslides. It is essential to implement appropriate land management practices to reduce the vulnerability to landslides, which is necessary to lessen the likelihood of landslide effects occurring, especially during monsoon seasons. Hence, it is essential to implement mitigating measures such as early notification systems and relocation strategies to guarantee the well-being of the people who live in the area.

IV. METHODOLOGY

A. Real-time monitoring system

The main factor causing the landslides in the area is incessant heavy rain in the area. The site selected for mon-

itoring is located in Mawiong Rim, which is on the NH-6, Guwahati Shillong (GS) road, Meghalaya, India (Fig. 2). Understanding the mechanism of slope failure due to rainfall is crucial because the behaviour of soil stress is altered by rain penetration on the slope to the extent that soil shear strength is outperformed. The geotechnical properties of the soil, precipitation, any vegetation that may or may not be present, hydrological parameters, etc., all impact how a slope behaves. The existence of tension fractures around the slope during the rainy season makes it simple for rainwater to infiltrate when it rains.

The real-time monitoring system is set up for an extended period to enable the study of the effects of rain on the slope for more than one year. A monitoring system has been installed to monitor the slope's behaviour throughout the dry and wet monsoon seasons. One can better comprehend how the slope reacts to rainfall if we keep a close eye on the soil's hydrological behaviour, the geotechnical characteristics of the slope, and the local precipitation. Sensors are placed around the selected slope at Mawiong Rim to track the matric suction, groundwater changes, slope displacement, and how rain affects them. Site excavation was performed in May 2021, where boreholes were prepared for installing a VW (vibrating wire) piezometer and VW inclinometer for real-time monitoring of GWT variation and slope displacement, respectively. The installed VW inclinometer is a bidirectional sensor (A+ A- and B+ B-) that gives readings along two directions. The upper sensor (A+ A-) recorded the tilt angles along the southeast (SE) direction, and the lower sensor (B+ B-) along the southwest (SW) direction (Fig. 2). Three bi-directional vibrating wire (VW) vertical multi-point inclinometers have been used to measure horizontal displacements along various points on the borehole (10 m, 20 m and 30 m). The VW piezometer is a pressure sensor that gives readings based on the pressure it detects at its top. Tensiometers are used to monitor matric suction (negative pore water pressure). The range of the sensor is 50 kg/cm³. The readings are obtained in centibar (10-2/1 kPa), and the sensor range is 200 centibar. Three watermark sensors (I1, I2, I3) have been installed along the slope below the ground surface. A rain gauge monitors the rainfall duration and intensity (Fig. 2). With a data logger intensity, the sensors' data are gathered and sent (Fig. 2). The data logger may hold up to 512 MB of data & a macro-size SIM card is inserted inside it. Data are received, collected and transferred to an email account using the internet connection from the SIM card provided (Fig. 2)

B. Bi-directional LSTM

Two independent LSTM layers, one processing the input sequence in the forward direction and the other in the reverse direction are combined to obtain the required performance. Starting with the first time step and moving forward sequentially through the next time steps, the forward LSTM layer processes the input stream to the end. Each LSTM cell estimates an output and a fresh hidden state at each time step, using the input and the previous hidden state as inputs. Each time-step's output is used as input for the one after it.

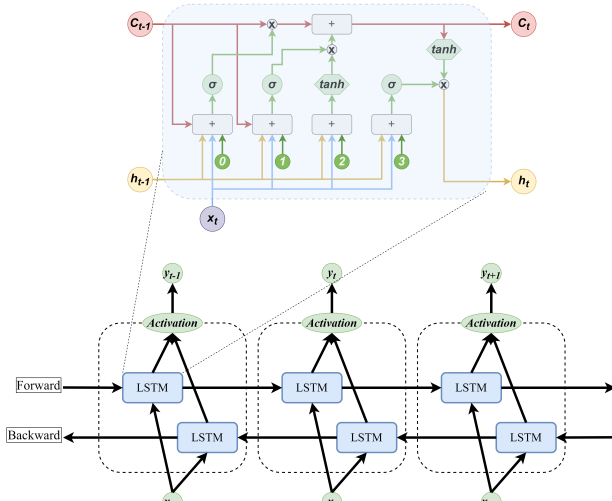


Fig. 3: Structure of LSTM and Bi-LSTM

The reverse LSTM layer processes the input sequence in the opposite direction, going from the most recent time step back to the initial time step. Similarly, it computes an output and a new hidden state for each time step using the input and the previous hidden state. Each time step provides its output as input to the one before it. The outputs of corresponding time steps from both directions are concatenated once the forward and reverse LSTM layers have processed the whole input sequence. The outcome is a final representation containing data from each time step's past and future contexts. The model may capture dependencies and patterns in both directions owing to the concatenation. The subsequent layers or the output layer directly receive the concatenated output representation from the bi-directional LSTM layers for prediction and further computation.

Given a series of input $\tilde{\mathbf{X}} = (x_1, x_2, \dots, x_T)$, a standard recurrent neural network (RNN) produces the hidden vector sequence, $\tilde{\mathbf{h}} = (h_1, h_2, \dots, h_T)$ and output vector sequence $\tilde{\mathbf{Y}} = (y_1, y_2, \dots, y_T)$, by iterating the following expressions for $t = [1, T]$:

$$\tilde{\mathbf{h}}_t = H(\tilde{\mathbf{W}}_{x_y h_t} + \tilde{\mathbf{W}}_{h_k h_t} - \tilde{\mathbf{b}}_h) \quad (1)$$

$$\tilde{\mathbf{y}}_t = \tilde{\mathbf{W}}_{h_y h_t} + \tilde{\mathbf{b}}_y \quad (2)$$

where H is the hidden layer function, the \mathbf{W} terms represent weight matrices (for example, \mathbf{W}_{x_h} is the input hidden weight matrix), and the b terms denote bias vectors (for example, \mathbf{b}_h is the hidden bias vector). H is usually an element-wise application of a predefined activation function (e.g., Sigmoid, Tanh, ReLu, etc.). The LSTM architecture, which uses memory cells to retain information, is shown to be more effective at calculating and using long-range context. The composite function specified by: is used to implement H in the LSTM version of this work.

$$i_t = \tanh(\tilde{\mathbf{W}}_{x_f x_t} + \tilde{\mathbf{W}}_{h_f h_t} - \tilde{\mathbf{W}}_{c_f c_t} - \tilde{\mathbf{b}}_i) \quad (3)$$

$$f_t = \tanh(\tilde{\mathbf{W}}_{x_f x_t} + \tilde{\mathbf{W}}_{h_f h_{t-1}} + \tilde{\mathbf{W}}_{c_f c_{t-1}} + \tilde{\mathbf{b}}_f) \quad (4)$$

$$f_t = f_t c_t - \tanh(\tilde{\mathbf{W}}_{x_c x_t} + \tilde{\mathbf{W}}_{h_c h_{t-1}} + \tilde{\mathbf{b}}_c) \quad (5)$$

Algorithm 1 Bi-directional LSTM for landslide prediction

Require: train-test-split (\vec{X}, \vec{Y})

Ensure: Predictions

Define the model

function $LSTM(x, h, c, \tilde{\mathbf{W}}, \tilde{\mathbf{U}}, \tilde{\mathbf{b}})$

$$\tilde{\mathbf{f}} \leftarrow \sigma(\tilde{\mathbf{W}}_f x + \tilde{\mathbf{U}}_f h + \tilde{\mathbf{b}}_f)$$

$$\tilde{\mathbf{i}} \leftarrow \sigma(\tilde{\mathbf{W}}_i x + \tilde{\mathbf{U}}_i h + \tilde{\mathbf{b}}_i)$$

$$\tilde{\mathbf{o}} \leftarrow \sigma(\tilde{\mathbf{W}}_o x + \tilde{\mathbf{U}}_o h + \tilde{\mathbf{b}}_o)$$

$$\tilde{\mathbf{c}}' \leftarrow \tanh(\tilde{\mathbf{W}}_c x + \tilde{\mathbf{U}}_c h + \tilde{\mathbf{b}}_c)$$

$$\tilde{\mathbf{c}} \leftarrow \tilde{\mathbf{f}} \odot \tilde{\mathbf{c}} + \tilde{\mathbf{i}} \odot \tilde{\mathbf{c}}'$$

$$\tilde{\mathbf{h}} \leftarrow \tilde{\mathbf{o}} \odot \tanh(\tilde{\mathbf{c}})$$

return \mathbf{h}, \mathbf{c}

function $BiLSTM(\tilde{\mathbf{X}})$

$$\tilde{\mathbf{H}} \leftarrow \{\}, \tilde{\mathbf{C}} \leftarrow \{\}$$

for x **in** $\tilde{\mathbf{X}}$ **do**

$$\tilde{\mathbf{h}}_f, \tilde{\mathbf{c}}_f \leftarrow LSTM(x, \tilde{\mathbf{h}}_f, \tilde{\mathbf{c}}_f, \tilde{\mathbf{W}}_f, \tilde{\mathbf{U}}_f, \tilde{\mathbf{b}}_f)$$

$$\tilde{\mathbf{H}} \leftarrow \tilde{\mathbf{H}} \cup \{\mathbf{h}_f\}$$

$$\tilde{\mathbf{C}} \leftarrow \tilde{\mathbf{C}} \cup \{\mathbf{c}_f\}$$

$$\tilde{\mathbf{H}}_b \leftarrow \{\}, \tilde{\mathbf{C}}_b \leftarrow \{\}$$

for x **in** $\text{reverse}(\tilde{\mathbf{X}})$ **do**

$$\tilde{\mathbf{h}}_b, \tilde{\mathbf{c}}_b \leftarrow LSTM(x, \tilde{\mathbf{h}}_b, \tilde{\mathbf{c}}_b, \tilde{\mathbf{W}}_b, \tilde{\mathbf{U}}_b, \tilde{\mathbf{b}}_b)$$

$$\tilde{\mathbf{H}}_b \leftarrow \{\mathbf{h}_b\} \cup \tilde{\mathbf{H}}_b$$

$$\tilde{\mathbf{C}}_b \leftarrow \{\mathbf{c}_b\} \cup \tilde{\mathbf{C}}_b$$

$$\tilde{\mathbf{H}} \leftarrow \text{concatenate}(\tilde{\mathbf{H}}, \tilde{\mathbf{H}}_b)$$

$$\tilde{\mathbf{C}} \leftarrow \text{concatenate}(\tilde{\mathbf{C}}, \tilde{\mathbf{C}}_b)$$

return $\tilde{\mathbf{H}}, \tilde{\mathbf{C}}$

Evaluate the model on test data & produce prediction graphs

$$o_t = \tanh(\tilde{\mathbf{W}}_{x_o x_t} + \tilde{\mathbf{W}}_{h_o h_{t-1}} + \tilde{\mathbf{W}}_{c_o c_t} + \tilde{\mathbf{b}}_o) \quad (6)$$

$$h_t = o_t * \tanh(\tilde{\mathbf{c}}_t) \quad (7)$$

Where, h is the hidden vector, \tanh is the hyperbolic tangent function, and I , f , o , and c are the input gate, forget gate, output gate, and cell activation vectors, respectively. Only element m of the cell vector is accepted as an input by the weight matrices that connect the cell to the gate vector. Uni-directional neural networks lack the fact that they can make use of the previous context only. As illustrated in (2), a bi-directional neural network computes the forward hidden sequence($\tilde{\mathbf{h}}_+$), the backward hidden sequence ($\tilde{\mathbf{h}}_-$), and the output sequence $\tilde{\mathbf{Y}}$ by iterating the backward layer from $t = T$ to 1, the forward layer from $t = 1$ to T , and then updating the output layer:

$$\tilde{\mathbf{h}}_+ = \tilde{\mathbf{H}}(\tilde{\mathbf{W}}_{x_h} + \mathbf{x}_t + \tilde{\mathbf{W}}_h + \mathbf{h}_+ + \mathbf{h}_{t-1} + \tilde{\mathbf{b}}_{h+}) \quad (8)$$

$$\tilde{\mathbf{h}}_- = \tilde{\mathbf{H}}(\tilde{\mathbf{W}}_{x_h} - \mathbf{x}_t + \tilde{\mathbf{W}}_h - \mathbf{h}_- + \mathbf{h}_{t+1} + \tilde{\mathbf{b}}_{h-}) \quad (9)$$

$$\tilde{\mathbf{y}}_t = 2 * \tilde{\mathbf{W}}_h + \tilde{\mathbf{y}}_{h+} - \mathbf{y}_{h-} + \tilde{\mathbf{b}}_{h-} \quad (10)$$

The combination bi-directional neural network with LSTM gives Bi-directional LSTM and hence may acquire lengthy contexts in either way of input. Three models have been prepared using bi-directional LSTM to predict slope deflections along SE and SW directions, matric suction and changing GWT separately. For predicting slope tilt angles, rainfall

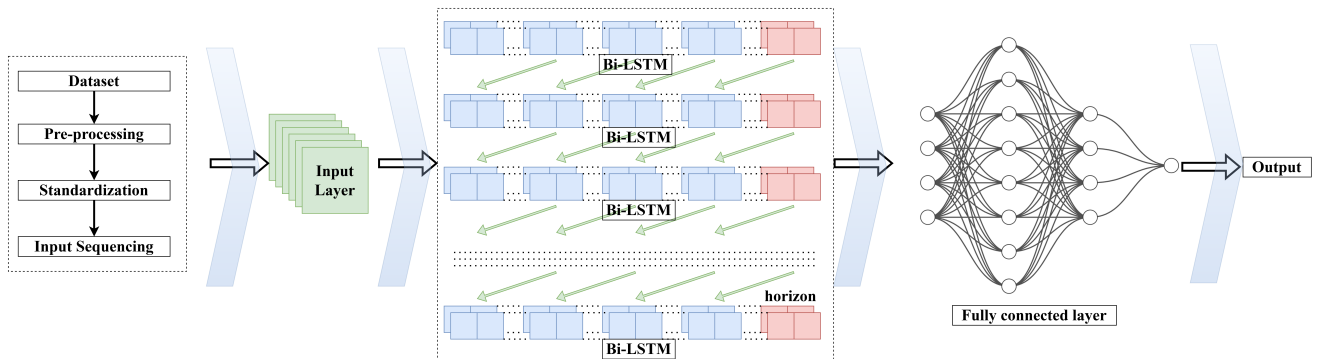


Fig. 4: Framework of the proposed Bi-LSTM based prediction model

TABLE I: Parameters of the model for slope displacement and matric suction

Parameter	Inclinometer depth and orientation								Matric suction and water level						
	30m (INC-30U)	up	30m (INC-30D)	down	20m (INC-20U)	up	20m (INC-20D)	down	10m (INC-10U)	up	10m (INC-10D)	down	MS1 (I1)	MS2 (I2)	MS3 (I3)
Input Unit	512	192	512	512	32	96			448	320	352	256			
Number of layers	4	4	4	4	4	4			4	1	2	1			
LSTM_0_units	512	64	32	32	512	448			416	64	192	352			
Layer_2_neurons	512	416	32	512	32	224			32	352	288	256			
Dropout rate	0.0	0.1	0.0	0.0	0.0	0.1			0.3	0.2	0.2	0.0			
Dense activation	tanh	tanh	ReLU	ReLU	ReLU	ReLU			tanh	tanh	ReLU	tanh			
LSTM_1_units	32	32	32	32	32	32			32	128	32	32			
LSTM_2_units	32	32	32	32	32	32			32	32	32	32			
LSTM_3_units	32	32	32	32	32	32			32	32	32	32			
MSE	0.0003188	0.005424	0.002544	0.00617	0.001882	0.002568			0.002302	6.68E-06	0.003346	0.000406			
R2 score	0.91	0.90	0.91	0.91	0.91	0.92			0.95	0.99	0.91	0.99			

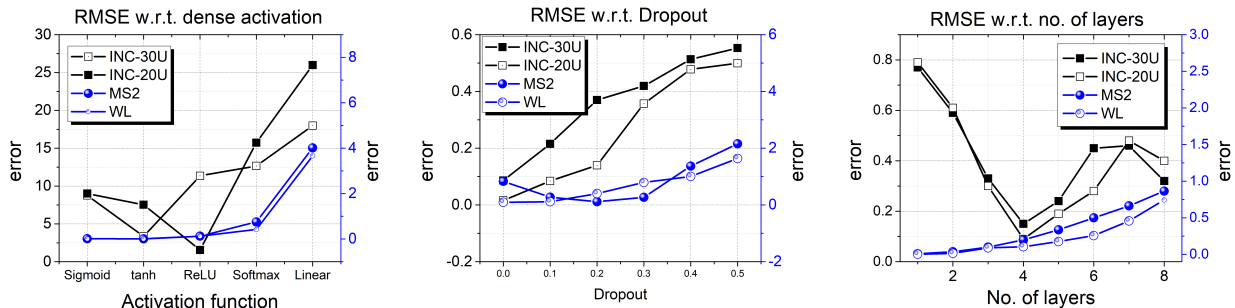


Fig. 5: Parameter tuning in the proposed model in slope displacement and matric suction

patterns, matric suction, GWT variation, and time are taken as the inputs. For slope displacement, six models have been prepared (INC-30U, INC-30D, INC-20U, INC-20D, INC-10U, INC-10D). Matric suction has been predicted using rainfall patterns, GWT variation, and time as the input parameters, and a total of three models have been developed (MS1, MS2, MS3). Whereas the variation in GWT has been predicted using rainfall patterns with time, a single model has been developed (WL). The dataset used for modelling is from 21st August 2022 to 16th January 2023. After data normalization, the data is split into three sets for training and testing, defined as 75%, and 25%, respectively. To do the split train test, the split function under sklearn has been used. This function randomly makes the partition and creates the data.

V. RESULTS AND DISCUSSION

To check the error of the model, mean square error (MSE), which is the average of the square of the difference between the actual and the predicted values of the variable, is observed.

The inaccuracy increases with the increasing numbers. An indicator of how much variation for a dependent variable can be explained by an independent variable is called R-squared (R2). R2 evaluates a model's goodness of fit. Therefore, a higher R2 value denotes a good fit, whereas a lower R2 denotes a poor fit for the model. The displacements are given by the inclinometers, which are placed below the ground at depths of 10m, 20m and 30m. These inclinometers give two sets of data along SE (southeast) and SW (southwest) directions; therefore, six displacements are obtained. After reading the dataset, only the required input and target variables are filtered. The input variables for predicting slope displacements (INC) are rainfall, water pressure, water level, time and matrix suction. Rainfall and time are used as inputs for the prediction of the Matrix Suction (MS).

A. Predictive models

The values of the various parameters that the models used to predict the soil movement in the datasets are shown in

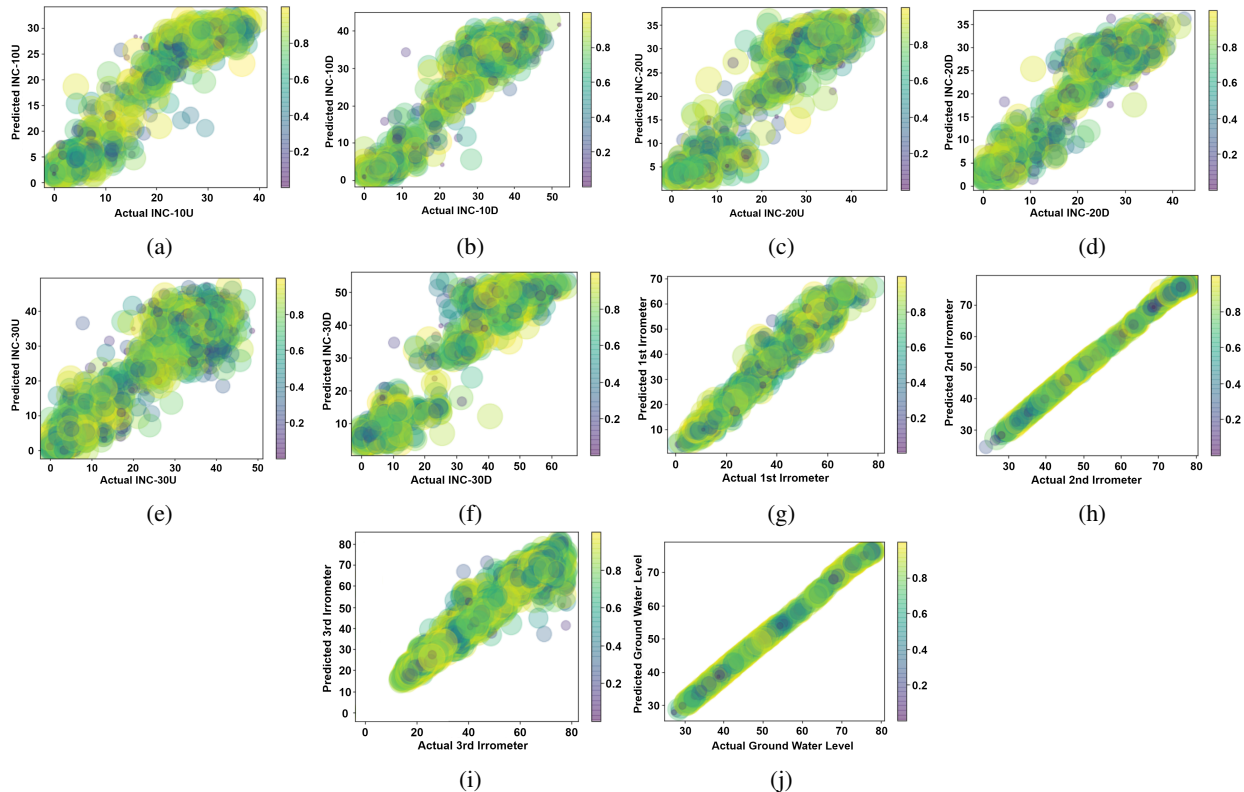


Fig. 6: Correlation between actual and predicted values (a) INC-10U, (b) INC-10D, (c) INC-20U, (d) INC-20D, (e) INC-30U, (f) INC-30D, (g) Matric suction 1, (h) Matric suction 2, (i) Matric suction 3, and (j) Ground Water Level

Table I. The number of units that define the dimension of hidden states or outputs and the number of parameters in the LSTM layer are 512 for INC-30U, INC-20U and INC-20D; 192 for INC-30D and 32 for INC-10U; 96 for INC-10D. All the models have 4 layers each: one input layer, two hidden layers and one output layer. The data compares several LSTM layer-based training settings for deep learning models (Fig. 6). Layer count, LSTM unit count, neurons in each layer, dropout rate, activation function, and batch size for training are among the factors. The mean squared error and R2 score represent the training outcomes. According to the findings, the model with the most LSTM units and layers and the greatest dropout rate had the lowest mean squared error (MSE) and highest R2 score. According to this, the best model for this dataset is the one with the most layers, LSTM units, and dropout rates. The findings were also influenced by the activation function employed for the dense layer, with the tanh activation function outperforming the ReLU activation function. As all the models had comparable values for these two parameters, the epochs and batch size did not affect the outcomes. The findings indicate that the model with the most LSTM units and layers and the greatest dropout rate is the best model for this dataset. The activation function used for the dense layer also impacts the results, with the tanh activation function outperforming the ReLU activation function. As all the models had comparable values for these two parameters, the epochs and batch size did not affect the outcomes. The activation technique in a neural network converts the entire weighted

input of the node into activation of the node or output for that input. A piecewise linear transformation called the rectified linear activation function (ReLU) outputs 0 when the input is negative and the input straight away when it is positive. It has developed into the default activation function for many different types of neural networks since a model using it is easier to train and typically performs better. The vanishing gradient phenomenon prevents the application of the sigmoid and hyperbolic tangent activation functions in networks with numerous layers. The vanishing gradient issue is fixed by the ReLU function, which enables models to learn more quickly and perform better. It is the default activation when creating multilayer Perceptron and convolutional neural networks.

The model showed an overall accuracy of 95.9% on the training data and an accuracy of 93% on the test data, as in Table II. The model correctly predicted the 10m, 20m, and 30m up and down slope displacements (Fig. 6a-6f) as well as the 1st, 2nd, and 3rd irrrometer measurements (Fig. 6g-6i) and water level (Fig. 6j).

The model's results demonstrate that it is highly accurate and can learn from the data and make accurate predictions. It was able to accurately forecast the tilt degree of the landslide across a wide range of groundwater levels, matric suction, and rainfall scenarios. The data compares several LSTM layer-based training settings for deep learning models, with the mean squared error and R2 score representing the training outcomes. The model used an LSTM network to learn the input data and output the predicted soil slope water level.

TABLE II: Comparison between the previous model and the proposed work for predicting slope displacement and matric suction

Reference	Prediction Model	Training		Testing	
		R2	RMSE	R2	RMSE
[31]	CNN with Moth frame logarithm	-	-	0.80	0.3685
[32]	CNN	-	-	-	9.97
[33]	RNN and CNN	-	-	0.88	0.083
[34]	Adtree, BAA DT, RSADT, RFADT	-	-	0.93	0.397
[35]	ABSGD	-	-	0.77	0.411
[36]	Xgboost	-	-	0.89	-
[37]	SIGMA	-	-	0.79	-
[38]	CNN	-	-	0.86	0.14
	ANN	-	-	0.71	1.45
	KNN	-	-	0.68	2.27
	SVR	-	-	0.59	2.53
	Decision tree	-	-	0.72	2.7
	Lasso	-	-	0.61	2.5
	LR	-	-	0.58	2.31
Proposed model	INC- 30U Bi-LSTM	0.93	0.0018	0.91	0.0032
	INC- 30D Bi-LSTM	0.94	0.0011	0.91	0.0054
	INC- 20U Bi-LSTM	0.94	0.0018	0.90	0.0025
	INC- 20D Bi-LSTM	0.96	0.0028	0.91	0.0062
	INC- 10U Bi-LSTM	0.95	0.0009	0.91	0.0019
	INC- 10D Bi-LSTM	0.96	0.0010	0.92	0.0026
	MS1 Bi-LSTM	0.97	0.0018	0.95	0.0025
	MS2 Bi-LSTM	0.99	0.0028	0.99	0.0062
	MS3 Bi-LSTM	0.96	0.0009	0.91	0.0019
	WL Bi-LSTM	0.99	0.0010	0.99	0.0026

The matric suction models provided useful insights into the soil moisture content of the roadside soil, allowing for better decision-making regarding water management. The model accurately predicted the seasonal fluctuations in water levels, which showed that the water levels reached their maximum peaks in the summer and their lowest levels in the winter. This demonstrated that the groundwater system was dynamic and adaptable to the ever-shifting external circumstances. The model indicated optimism about groundwater levels in the months ahead.

B. Comparative analysis

TABLE III: Comparison of the proposed model with LSTM and Bi-LSTM models in the landslide dataset

Model	Parameter	Training		Testing	
		R2	RMSE	R2	RMSE
LSTM	INC-30U	0.74	0.1011	0.68	0.1567
	INC-30D	0.71	0.1172	0.52	0.1934
	INC-20U	0.70	0.1218	0.66	0.1841
	INC-20D	0.55	0.2374	0.51	0.2458
	INC-10U	0.69	0.1882	0.45	0.2687
	INC-10D	0.52	0.2555	0.51	0.2604
	MS1	0.66	0.2053	0.64	0.1937
	MS2	0.45	0.3014	0.44	0.3387
	MS3	0.51	0.2672	0.47	0.3155
	WL	0.68	0.1672	0.49	0.2288
Bi-LSTM	INC-30U	0.86	0.0101	0.81	0.0664
	INC-30D	0.89	0.0056	0.86	0.0083
	INC-20U	0.88	0.0071	0.85	0.0098
	INC-20D	0.79	0.0107	0.76	0.0276
	INC-10U	0.87	0.0025	0.83	0.0170
	INC-10D	0.90	0.0029	0.89	0.0091
	MS1	0.84	0.0080	0.81	0.0110
	MS2	0.92	0.0130	0.91	0.0208
	MS3	0.91	0.0094	0.90	0.0107
Proposed work	WL	0.93	0.0070	0.91	0.0098
	INC-30U	0.93	0.0018	0.91	0.0032
	INC-30D	0.94	0.0011	0.91	0.0054
	INC-20U	0.94	0.0018	0.9	0.0025
	INC-20D	0.96	0.0028	0.91	0.0062
	INC-10U	0.95	0.0009	0.91	0.0019
	INC-10D	0.96	0.001	0.92	0.0026
	MS1	0.97	0.0018	0.95	0.0025
	MS2	0.99	0.0028	0.99	0.0062
	MS3	0.96	0.0009	0.91	0.0019
	WL	0.99	0.001	0.99	0.0026

The metrics in Table III show a comparison of the proposed model with its predecessor LSTM and Bi-LSTM models implemented on the same dataset. The auto-regressive component of the model incorporates its previous predictions as inputs for making subsequent predictions. This incorporates feedback derived from prior predictions into the modelling procedure. In contrast to LSTM and Bi-LSTM models, which are commonly utilized for univariate sequences, an auto-regressive multivariate Bi-LSTM architecture is specifically developed to accommodate multivariate data, wherein each time step can encompass multiple features or variables. This enables the capturing of relationships among multiple factors concurrently. The model can capture the spatial and temporal dependencies of the data. The proposed method utilizes bidirectional context to account for temporal dependencies and incorporates multivariate features to capture spatial relationships. The proposed approach in machine learning is the auto-regressive multivariate Bi-LSTM, designed to produce multiple outputs at each time step. Each of these outputs corresponds to a predicted variable. This characteristic renders it highly suitable for forecasting multivariate time series data. The auto-regressive multivariate Bi-LSTM is a sophisticated model that integrates bidirectional modelling, multivariate feature handling, and auto-regressive feedback to enhance the accuracy of predictions for multivariate temporal data.

VI. CONCLUSION

This method uses deep learning and focuses on actively predicting periodic displacement due to local precipitation.

- There is a good agreement between the measured and anticipated deformation values.
- The findings imply that rainfall is the most significant dynamic and numerous elements influencing the deformation of the slope displacement in the Mawiong Rim landslide.
- The bi-directional LSTM model and concept offer a potentially effective means of improving the effectiveness and precision of the landslide warning system on the ground ([18], [19]). The bi-directional LSTM model can be used to predict the slope displacement, the matric suction, and water level using INC-Model, MS-Model, and WL-Model, respectively.
- An economical tool is developed for predicting soil slope instability at a local scale level. The models developed predict slope displacements, matric suction, and GWL. The models developed did not require soil parameters or geometrical data to accurately predict the GWL, matric suction, and slope displacement. Hence, these models can be easily applied to any other area, knowing the site's initial water level, matric suction, and rainfall patterns.
- Past research shows that most of them have high accuracy levels but also high root mean square errors. Hence, this shows that the prediction models may have high errors while predicting the landslide phenomenon. Therefore, the current study gives highly accurate predictions and shallow errors in predicting landslides or slope displacements.

Funding/Acknowledgement: This work was supported by the DST SERB, Govt. of India; (ECR/2018002807) and DST International Bilateral Co-operation Division, Govt. of India (DST/INT/JSPS/P301/2019)

REFERENCES

- [1] M.-G. Angeli, A. Pasuto, and S. Silvano, "A critical review of landslide monitoring experiences," *Engineering Geology*, vol. 55, no. 3, pp. 133–147, 2000.
- [2] R. Greco, A. Guida, E. Damiano, and L. Olivares, "Soil water content and suction monitoring in model slopes for shallow flowslides early warning applications," *Physics and Chemistry of the Earth, Parts A/B/C*, vol. 35, no. 3-5, pp. 127–136, 2010.
- [3] H. Rahardjo, A. S. Nio, F. R. Harnas, and E. C. Leong, "Comprehensive instrumentation for real time monitoring of flux boundary conditions in slope," *Procedia Earth and Planetary Science*, vol. 9, pp. 23–43, 2014.
- [4] K. Das, S. Majumdar, S. Moulik, and M. Fujita, "Real-time threshold-based landslide prediction system for hilly region using wireless sensor networks," in *2020 IEEE International Conference on Consumer Electronics-Taiwan (ICCE-Taiwan)*. IEEE, 2020, pp. 1–2.
- [5] S. Li, J. He, Y. Li, and M. U. Rafique, "Distributed recurrent neural networks for cooperative control of manipulators: A game-theoretic perspective," *IEEE transactions on neural networks and learning systems*, vol. 28, no. 2, pp. 415–426, 2016.
- [6] L. Jin, X. Zheng, and X. Luo, "Neural dynamics for distributed collaborative control of manipulators with time delays," *IEEE/CAA Journal of Automatica Sinica*, vol. 9, no. 5, pp. 854–863, 2022.
- [7] W. Yang, S. Li, Z. Li, and X. Luo, "Highly-accurate manipulator calibration via extended kalman filter-incorporated residual neural network," *IEEE Transactions on Industrial Informatics*, 2023.
- [8] X. Luo, Y. Zhong, Z. Wang, and M. Li, "An alternating-direction-method of multipliers-incorporated approach to symmetric non-negative latent factor analysis," *IEEE Transactions on Neural Networks and Learning Systems*, 2021.
- [9] H. Salehi, S. Das, S. Biswas, and R. Burgueño, "Data mining methodology employing artificial intelligence and a probabilistic approach for energy-efficient structural health monitoring with noisy and delayed signals," *Expert Systems with Applications*, vol. 135, pp. 259–272, 2019.
- [10] D. Wu, X. Luo, Y. He, and M. Zhou, "A prediction-sampling-based multilayer-structured latent factor model for accurate representation to high-dimensional and sparse data," *IEEE Transactions on Neural Networks and Learning Systems*, 2022.
- [11] F. Huang, J. Huang, S. Jiang, and C. Zhou, "Landslide displacement prediction based on multivariate chaotic model and extreme learning machine," *Engineering Geology*, vol. 218, pp. 173–186, 2017.
- [12] A. Graves, S. Fernández, and J. Schmidhuber, "Bidirectional lstm networks for improved phoneme classification and recognition," in *Artificial Neural Networks: Formal Models and Their Applications-ICANN 2005: 15th International Conference, Warsaw, Poland, September 11-15, 2005. Proceedings, Part II 15*. Springer, 2005, pp. 799–804.
- [13] K. Greff, R. K. Srivastava, J. Koutník, B. R. Steunebrink, and J. Schmidhuber, "Lstm: A search space odyssey," *IEEE transactions on neural networks and learning systems*, vol. 28, no. 10, pp. 2222–2232, 2016.
- [14] Y. Xing, J. Yue, C. Chen, K. Cong, S. Zhu, and Y. Bian, "Dynamic displacement forecasting of dashuitian landslide in china using variational mode decomposition and stack long short-term memory network," *Applied sciences*, vol. 9, no. 15, p. 2951, 2019.
- [15] B. Yang, K. Yin, S. Lacasse, and Z. Liu, "Time series analysis and long short-term memory neural network to predict landslide displacement," *Landslides*, vol. 16, pp. 677–694, 2019.
- [16] H. Li, Q. Xu, Y. He, and J. Deng, "Prediction of landslide displacement with an ensemble-based extreme learning machine and copula models," *Landslides*, vol. 15, pp. 2047–2059, 2018.
- [17] C. Lian, L. Zhu, Z. Zeng, Y. Su, W. Yao, and H. Tang, "Constructing prediction intervals for landslide displacement using bootstrapping random vector functional link networks selective ensemble with neural networks switched," *Neurocomputing*, vol. 291, pp. 1–10, 2018.
- [18] K. Zhang, K. Zhang, C. Cai, W. Liu, and J. Xie, "Displacement prediction of step-like landslides based on feature optimization and vmd-bi-lstm: a case study of the bazimen and baishuihe landslides in the three gorges, china," *Bulletin of Engineering Geology and the Environment*, vol. 80, pp. 8481–8502, 2021.
- [19] P. Kumar, P. Sihag, P. Chaturvedi, K. Uday, and V. Dutt, "Bs-lstm: an ensemble recurrent approach to forecasting soil movements in the real world," *Frontiers in Earth Science*, vol. 9, p. 696792, 2021.
- [20] F. A. Gers, J. Schmidhuber, and F. Cummins, "Learning to forget: Continual prediction with lstm," *Neural computation*, vol. 12, no. 10, pp. 2451–2471, 2000.
- [21] Q. Meng, H. Wang, M. He, J. Gu, J. Qi, and L. Yang, "Displacement prediction of water-induced landslides using a recurrent deep learning model," *European Journal of Environmental and Civil Engineering*, pp. 1–15, 2020.
- [22] X. Li, J. Kong, and Z. Wang, "Landslide displacement prediction based on combining method with optimal weight," *Natural Hazards*, vol. 61, pp. 635–646, 2012.
- [23] C. Zhou, K. Yin, Y. Cao, and B. Ahmed, "Application of time series analysis and pso-svm model in predicting the bazimen landslide in the three gorges reservoir, china," *Engineering geology*, vol. 204, pp. 108–120, 2016.
- [24] C. Lian, Z. Zeng, W. Yao, H. Tang, and C. L. P. Chen, "Landslide displacement prediction with uncertainty based on neural networks with random hidden weights," *IEEE transactions on neural networks and learning systems*, vol. 27, no. 12, pp. 2683–2695, 2016.
- [25] Y.-T. Tsai, Y.-R. Zeng, and Y.-S. Chang, "Air pollution forecasting using rnn with lstm," in *2018 IEEE 16th Intl Conf on Dependable, Autonomic and Secure Computing, 16th Intl Conf on Pervasive Intelligence and Computing, 4th Intl Conf on Big Data Intelligence and Computing and Cyber Science and Technology Congress (DASC/PiCom/DataCom/CyberSciTech)*. IEEE, 2018, pp. 1074–1079.
- [26] P. Xie, A. Zhou, and B. Chai, "The application of long short-term memory (lstm) method on displacement prediction of multifactor-induced landslides," *IEEE Access*, vol. 7, pp. 54 305–54 311, 2019.
- [27] M. K. Nammous, K. Saeed, and P. Kobojek, "Using a small amount of text-independent speech data for a bilstm large-scale speaker identification approach," *Journal of King Saud University-Computer and Information Sciences*, vol. 34, no. 3, pp. 764–770, 2022.
- [28] E. Brand, "Some thoughts on rain-induced slope failures," in *Proc. 10th ICSMFE*, vol. 3, 1981, pp. 373–376.
- [29] A. Graves, "Generating sequences with recurrent neural networks," *arXiv preprint arXiv:1308.0850*, 2013.
- [30] M. Boden, "A guide to recurrent neural networks and backpropagation," *the Dallas project*, vol. 2, no. 2, pp. 1–10, 2002.
- [31] V. D. Pham, Q.-H. Nguyen, H.-D. Nguyen, V.-M. Pham, Q.-T. Bui et al., "Convolutional neural network—optimized moth flame algorithm for shallow landslide susceptible analysis," *IEEE Access*, vol. 8, pp. 32 727–32 736, 2020.
- [32] H. Pei, F. Meng, and H. Zhu, "Landslide displacement prediction based on a novel hybrid model and convolutional neural network considering time-varying factors," *Bulletin of Engineering Geology and the Environment*, vol. 80, no. 10, pp. 7403–7422, 2021.
- [33] P. T. T. Ngo, M. Panahi, K. Khosravi, O. Ghorbanzadeh, N. Kariminejad, A. Cerda, and S. Lee, "Evaluation of deep learning algorithms for national scale landslide susceptibility mapping of iran," *Geoscience Frontiers*, vol. 12, no. 2, pp. 505–519, 2021.
- [34] D. Tien Bui, H. Shahabi, E. Omidiyar, A. Shirzadi, M. Geertsema, J. J. Clague, K. Khosravi, B. Pradhan, B. T. Pham, K. Chapi et al., "Shallow landslide prediction using a novel hybrid functional machine learning algorithm," *Remote Sensing*, vol. 11, no. 8, p. 931, 2019.
- [35] B. Thai Pham, A. Shirzadi, H. Shahabi, E. Omidiyar, S. K. Singh, M. Sahana, D. Talebpour Asl, B. Bin Ahmad, N. Kim Quoc, and S. Lee, "Landslide susceptibility assessment by novel hybrid machine learning algorithms," *Sustainability*, vol. 11, no. 16, p. 4386, 2019.
- [36] H. Wang, L. Zhang, K. Yin, H. Luo, and J. Li, "Landslide identification using machine learning," *Geoscience Frontiers*, vol. 12, no. 1, pp. 351–364, 2021.
- [37] M. T. Abraham, N. Satyam, N. Shreyas, B. Pradhan, S. Segoni, K. N. Abdul Maulud, and A. M. Alamri, "Forecasting landslides using sigma model: a case study from idukki, india," *Geomatics, Natural Hazards and Risk*, vol. 12, no. 1, pp. 540–559, 2021.
- [38] M. Khalili, L. Guerriero, M. Pouralizadeh, D. Calcaterra, and D. Di Martire, "Prediction of deformation caused by landslides based on graph convolution networks algorithm and dinsar technique," *ISPRS Annals of the Photogrammetry, Remote Sensing and Spatial Information Sciences*, vol. 10, pp. 391–397, 2023.